Journal of Sound and Vibration (1997) **201**(4), 473–489

THE COMPLETE IMAGE-SOURCE METHOD FOR THE PREDICTION OF SOUND DISTRIBUTION IN NON-DIFFUSE ENCLOSED SPACES

S. M. Dance and B. M. Shield

Acoustics Group, School of Engineering Systems and Design, South Bank University, London SE1 0AA, England

(*Received* 18 *January* 1996, *and in final form* 18 *September* 1996)

An image-source based computer model is presented for the prediction of sound distribution in non-diffuse fitted enclosed spaces, such as factories. The new model, CISM, was developed on the basis of the sound propagation predictions of the Ondet and Barbry RAYCUB model in laboratory and industrial spaces. CISM uses an optimum representation, based on the accuracy of the RAYCUB results, so that the prediction accuracy is maintained while run-time and data input requirements are reduced. The basis of CISM is described, and predictions for various configurations of a fitted laboratory space, an empty factory incorporating a single barrier and a theoretical space with absorptive patches are presented. For comparison, sound propagation measurements were obtained and RAYCUB derived models, RAYCUB-DIR and RAYCUB-DIR REDIR, were used to predict these sound levels. This work demonstrated that the CISM model is as accurate as the ray-tracing model RAYCUB in the described enclosed spaces. The advantages of the CISM model are a reduced run-time (for a typical factory, CISM is approximately ten times faster than RAYCUB-DIR) and reduced data input (CISM uses less than half the information required by RAYCUB-DIR).

1. INTRODUCTION

With the introduction of international legislation to protect employees at work, there is now a need for an accurate practical prediction model to aid in the calculation of noise exposure of workers in industrial environments. A computer model would enable an employer to rearrange the working environment or an architect to design an industrial unit meeting the new legislation, if necessary by the application of noise control measures.

For industrial halls, classical acoustic theory has been shown to be inappropriate, as the sound field was found to be non-diffuse [1]. Computer modelling has been used to predict sound distribution in factory spaces during the past 20 years; the Ondet and Barbry program, RAYCUB [2], has emerged as the most accurate computer model, with many authors [3–5], independently testing their own data to validate the model. The two disadvantages of the RAYCUB model are the run-time requirements and the extensive information necessary to represent an enclosed space.

In an attempt to overcome these shortcomings, a new model, the Complete Image-Source Method (CISM), has been written. CISM is an image source model which incorporates those representational features of RAYCUB, such as flexible zoning of fittings, absorptive patches and acoustic barriers, which have been found to have the most significant effect on prediction accuracy without compromising the run-time or data requirements [6].

0022–460X/97/140473 + 17 $25.00/0/sv960770

This paper builds on the simple image-source model [7] which includes a parallelepiped geometry, isotropically distributed fittings, an air absorption coefficient and sound source directivity, to describe in detail the CISM model which includes absorptive patches, totally sound absorbing barriers and unevenly distributed fittings.

CISM was compared to different versions of the RAYCUB model. For the laboratory and theoretical spaces, RAYCUB was used. For the barrier case, two extended versions of RAYCUB were used: RAYCUB-DIR, which includes sound source directivity and RAYCUB-DIR REDIR, which additionally models diffractional effects [8]. The results are presented in terms of sound propagation curves, average prediction differences, run-times and data file sizes.

2. THE CISM MODEL

The parallelepiped image-source method has been used for the prediction of sound distribution in factory spaces by Hodgson [1], Jovivic [9], Lindqvist [10], Kurze [11] and Dance *et al*. [12]. Arbitrarily shaped performance spaces have also been modelled by using the general image-source method, which has not previously been used for factory spaces [13, 14].

CISM is based on geometric acoustics which represents the sound emanating from a sound source as separate sound paths. Each sound path represents a unique combination of reflections from any of the room surfaces, up to a predefined maximum reflection order. The sound intensity attributed to a sound path can be diminished through surface absorption, absorption by the fittings, air absorption, and the distance travelled according to the inverse square law. A barrier will terminate the sound path and hence it will not contribute to the sound distribution.

The factors which were found to deliver the greatest increase in prediction accuracy for the minimum increase in input data for the RAYCUB model have been incorporated into CISM. These factors include floor-ceiling or gangway zoning, a simple parallelepiped geometry for the room, an air absorption coefficient and sound source directivity [6].

The parallelepiped image-source method uses pairs of parallel surfaces to define the room; each surface is denoted by CISM as either positive or negative. For example, the floor represents the negative surface of the floor/ceiling pairing, and hence the ceiling is the positive surface.

2.1. FITTINGS

The basic image-source method does not represent fittings, so an approach to simulate these was required. In previous image-source models by Hodgson [1], Jovicic [9], Lindqvist [10] and Kurze [11], the fittings were assumed to be isotropically distributed. Lemire and Nicolas [15] were the first to model fittings as a floor zone based on the average fitting height. Hodgson [16] found that the Lemire and Nicolas approach led to predictions which under-estimated sound levels in fitted rooms near the sound source.

Current image-source models have been validated in laboratory spaces, in which the fittings were distributed either isotropically [9] or uniformly across the entire floor area [15]. The RAYCUB model is capable of representing arbitrary fitting distributions.

CISM extends the Lemire and Nicolas model by dividing the space into three horizontal or vertical zones. The unevenness of the fitting distribution is typically caused by gangways, open areas in industrial spaces and the non-uniform vertical distribution of fittings. The difference between CISM and the Lemire and Nicolas model is the parameter used to define the density of the fittings. CISM uses the Kuttruff scattering frequency parameter, q [17], whereas the Lemire and Nicolas model appears to have no direct relation with q

and hence the predicted sound levels of the two models can differ significantly. The CISM fittings model is, however, incapable of representing the scattering of the sound, unlike the models of Ondet and Barbry [2], Jovicic [9] and Lindqvist [10], so that at large distances from the nearest sound source CISM becomes progressively less accurate. In addition, CISM cannot model the backscattering from fittings, which can increase the sound level if the sound source is close to the fittings [1].

The sound path attenuation due to fittings is represented by a factor based on the distance travelled inside the zone. In this way the fittings are modelled as a dense continuous medium, the density being determined by the scattering frequency, q, as defined by Kuttruff,

$$q = \sum_{F=1}^{N} S_F/4V, \tag{1}$$

where N is the number of fittings in the zone, S_F is the surface area of a fitting and V is the volume of the zone.

The attenuation coefficient due to the fittings in a zone, f_a, is given by

$$f_a = (1 - \alpha_F)^{|d_F| * q}, \tag{2}$$

where q is the scattering frequency of the zone, d_F is the distance travelled by the sound in the zone, as defined below, and α_F is the average absorption coefficient of the fittings in the zone.

The total fitting attenuation coefficient, f, is the product of the fitting attenuation coefficients of the individual zones. The distance the sound path travels in a zone, d_F, is calculated by first determining the distance in the zone travelled in the z direction, d_{F_z}, which is given by the equation

$$d_{F_z} = \begin{cases} \left.\begin{matrix} k * F_z + s_z, & P_- \\ k * F_z - s_z, & P_+ \end{matrix}\right\} k \text{ odd} \\ \left.\begin{matrix} (k-1) * F_z + s_z, & P_- \\ (k+1) * F_z - s_z, & P_+ \end{matrix}\right\} k \text{ even} \end{cases} \Bigg\} r_z \geqslant F_z$$
$$\begin{cases} \left.\begin{matrix} (k-1) * F_z + s_z + r_z, & P_- \\ (k+1) * F_z - s_z - r_z, & P_+ \end{matrix}\right\} k \text{ odd} \\ \left.\begin{matrix} k * F_z + s_z - r_z, & P_- \\ k * F_z - s_z + r_z, & P_+ \end{matrix}\right\} k \text{ even} \end{cases} \Bigg\} r_z < F_z \tag{3}$$

where k is the reflection order for the z pairing of surfaces, F_z is the average height of the fittings, s_z is the height of the source and r_z is the receiver height. P_- indicates that the first reflection was on the negative surface of the pairing and P_+ indicates that the positive surface was struck first.

In Figure 1 is shown a simplified two-dimensional example illustrating the calculation of d_{F_z}, where the source and receiver are both below the fitting height, F_z, and the sound first strikes the floor, P_-, and is reflected twice, so k is even. Hence line 7 of equation (3) is appropriate. The first reflection in the surface P_- creates the image-space, I'_{z-}, in which the first order image-source, *Source′*, is located. The image-space I''_{z+} is created to incorporate the image-source, *Source″*, created by the second order reflection. I'_{z+} has no image-source, as the surface first struck was negative.

Translation of the axial distance, d_{F_z}, into the radial distance, d_F, travelled inside the fitted zone is achieved through the application of simple geometry. Simple subtraction is used to calculate the distance travelled in a centrally fitted zone, f_{centre}.

2.2. MODELLING ABSORPTIVE PATCHES

The representation of absorptive patches in an image-source model was developed by Gibbs and Jones [7]. The Gibbs and Jones model was capable of representing one centrally located patch per surface; each surface could have an arbitrary associated absorption coefficient, although all patches must have the same absorption coefficient.

With the Gibbs and Jones model used as a basis, CISM has been developed to model any number of arbitrarily positioned and sized absorptive patches on any of the room surfaces. Each absorptive patch has an associated absorption coefficient. To illustrate the calculation within the model, the effect on the sound path of an absorptive patch located on the left wall of a room is detailed in the following equations.

The gradients of the image-path in three dimensions (G_x, G_y, G_z) are calculated from the image-source, s, with co-ordinates (s_x, s_y, s_z) to the receiver, r, with co-ordinates (r_x, r_y, r_z) as

$$G_x = (s_x - r_x)/d, \qquad G_y = (s_y - r_y)/d, \qquad G_z = (s_z - r_z)/d, \tag{4}$$

where d is the length of the direct line between the image-source and receiver.

The co-ordinates of the intersections of the sound paths with the image-surfaces are calculated as follows. The x co-ordinate, C_{x_j}, of the intersection of the jth reflection with the image-surface is given by

$$C_{x_{j=1,n_x}} = \left\{ \begin{array}{l} \left.\begin{array}{ll} -l_x * j - 1, & P_- \\ l_x * j - 1, & P_+ \end{array}\right\} n_x \text{ even} \\ \left.\begin{array}{ll} l_x * j - 1, & P_- \\ -l_x * j - 1, & P_+ \end{array}\right\} n_x \text{ odd} \end{array} \right\}, \tag{5}$$

where n_x is the reflection order, P_- and P_+ represent the plane first struck and l_x is the room length. From the C_{x_j}, the corresponding y and z co-ordinates C_{y_j}, and C_{z_j}, can be calculated as

$$C_{y_{j=1,n_x}} = G_y/G_x * (C_{x_j} - r_x) + r_y, \qquad C_{z_{j=1,n_x}} = G_z/G_x * (C_{x_j} - r_x) + r_z. \tag{6}$$

The parameters H_{y_j} and H_{z_j}, which take the values "true" or "false", are used to indicate whether the sound paths hit a patch in the y- or z- planes on the jth reflection. For example,

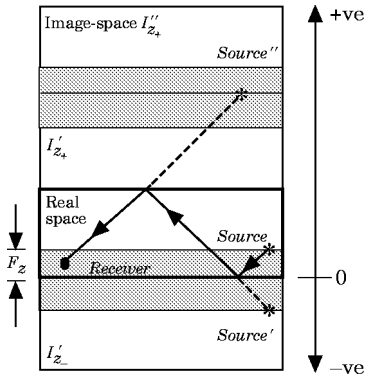

Figure 1. A simplified 2-D illustration of the fittings model in CISM.

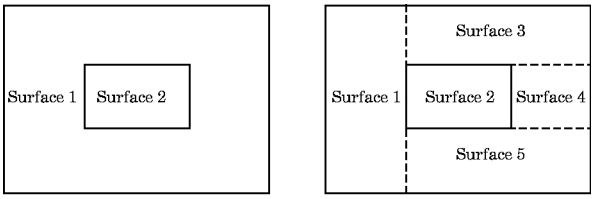

Figure 2. A room surface with an absorptive patch as represented by (a) CISM and (b) RAYCUB.

parameter H_{y_j} is given the value "true" if one of the following inequalities is satisfied, showing that the sound path hits the patch in the y plane on the jth reflection. Otherwise H_{y_j} takes the value "false".

$$\left\{\begin{array}{l}\left\{\begin{array}{ll}(C_{y_j}\backslash l_y) * l_y + P_{y_{min}} \leqslant C_{y_j} \leqslant (C_{y_j}\backslash l_y) * l_y + P_{y_{max}}, & (C_{y_j}\backslash l_y) \text{ even} \\ ((C_{y_j}\backslash l_y)+1) * l_y - P_{y_{max}} \leqslant C_{y_j} \leqslant ((C_{y_j}\backslash l_y)+1) * l_y - P_{y_{min}}, & (C_{y_j}\backslash l_y) \text{ odd}\end{array}\right\}, \quad C_{y_j} \geqslant 0 \\ \left\{\begin{array}{ll}(C_{y_j}\backslash l_y) * l_y - P_{y_{max}} \leqslant C_{y_j} \leqslant (C_{y_j}\backslash l_y) * l_y - P_{y_{\min}}, & (C_{y_j}\backslash l_y) \text{ even} \\ ((C_{y_j}\backslash l_y)-1) * l_y + P_{y_{min}} \leqslant C_{y_j} \leqslant ((C_{y_j}\backslash l_y)-1) * l_y + P_{y_{max}}, & (C_{y_j}\backslash l_y) \text{ odd}\end{array}\right\}, \quad C_{y_j} < 0\end{array}\right\}. \tag{7}$$

Here l_y and l_z are the dimensions of the room and $P_{y_{\min}}, P_{y_{\max}}, P_{z_{\min}}$ and $P_{z_{\max}}$ are the minimum and maximum boundaries of the patch. The symbol "$\backslash$" represents integer division. Hz_j is calculated similarly.

For each reflection order, if both H_y and H_z are true, then the sound path was reflected by the absorptive patch and the reflection coefficient, R_x, as used in the simple image-source equation [6], is multiplied by $(1 - \alpha_{patch})/(1 - \alpha_x)$, for the appropriate patch and room surface. The advantage of this approach is that the absorptive patch can be positioned over the room surface rather than dividing the entire room surface into separate patches; see Figure 2. In this way the data necessary to define a room is significantly reduced.

A simplified 2-D example is shown in Figure 3 to illustrate equations (5)–(8). The position of the image-source, as calculated in the simple image-source equation, is shown. The gradient of the sound path is calculated in equation (4), giving $G_x = -0{\cdot}8$ and $G_y = -0{\cdot}6$. Next, equation (5) is used to calculate the three crossing ordinates of the sound path and the X-axis, C_{x_1}, C_{x_2} and C_{x_3}, representing the reflection off the left wall. As three is odd and the first wall struck is denoted as negative, then line 1 of equation (5) was used to give $C_{x_1} = 0$, $C_{x_2} = -40$, $C_{x_3} = -80$ and $C_{x_4} = -120$. Equation (6) calculates the ordinates of the sound path as it crosses the Y-axis in the image-spaces, giving $C_{y_1} = 2{\cdot}5$, $C_{y_2} = -27{\cdot}5$, $C_{y_3} = -57{\cdot}5$ and $C_{y_4} = -87{\cdot}5$. By substituting these values into the inequalities (7), it can be shown that H_{y_1} and H_{y_3} take the value "true".

2.3. MODELLING TOTALLY ABSORPTIVE BARRIERS

A brief history is presented here of the modelling of barriers in image-source models during the past 20 years. Stehel and Braune [18] briefly detailed an image-source model capable of modelling barriers which could reflect sound from any room surface or barrier in a parallelepiped enclosed space, although no results were presented. The Kurze model [11] for barrier performance was validated in 54 shallow rooms, including both open-plan offices and industrial halls; the model was found to be accurate. Kurze predicted the barrier

performance by representing the direct shielding by the barrier and the sound striking the barrier as being scattered to all receivers. Kotarbinska [19] developed an image-source barrier reflection–diffraction model specifically for flat rooms; that is, only the floor, the ceiling and the barrier were modelled. This model was preliminarily verified in a 1:5 scale model and found to be reasonably accurate in two different experiments.

The CISM barrier model is based upon the absorptive patch model. The barrier can be modelled as an arbitrarily positioned and sized rectangular totally absorptive room surface, with a restriction on the barrier orientation that only barriers parallel to one of the six room surfaces can be modelled. As the absorptive patch must be located on one of the room surfaces a checking procedure was introduced to the absorptive patch model and a variable δ is introduced to indicate whether or not the barrier is struck. As the barrier is located inside the space two conditions need to be checked: first, if the highest order image-barrier is struck; and, second, if the "real" barrier is struck. In Figure 4 is shown an example of the workings of the barrier model. If the barrier is struck, δ is set to zero, and the sound does not contribute to the overall sound level at the receiver point of interest; otherwise, δ is set to one.

2.4. THE COMPLETE IMAGE-SOURCE METHOD

The complete model, CISM, implements the simple image-source equation [7] and extends the equation to include the elements detailed above. For each receiver point, the sound intensity is summed from all the sources, each of which produces sound paths that travel a unique route to the receiver by reflecting off the room surfaces, thereby attenuating the sound intensity by the appropriate reflection coefficient, R, which incorporates the absorptive patch attenuations, as described in section 2.2. This unique route has an associated directivity factor, Q, which adjusts the intensity associated with the sound. The sound intensity is also reduced by air attenuation as defined by the coefficient A. Finally, the sound has three possible fitted zones to travel through causing a total fittings

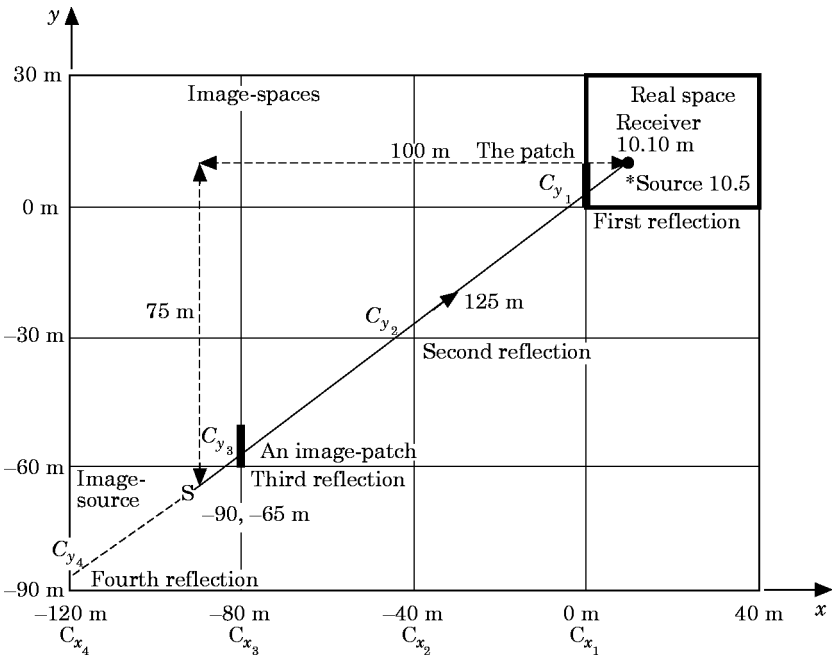

Figure 3. A simplified 2-D illustration of the CISM absorptive patch model.

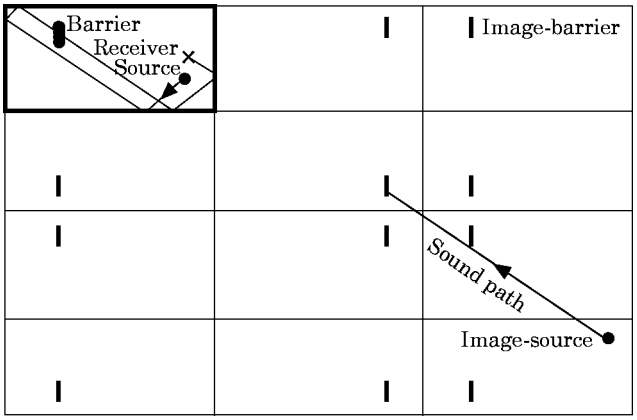

Figure 4. A simplified 2-D illustration of the CISM barrier model.

attenuation of f, as described in section 2.1. The resultant total sound level, L, at a particular receiver point is given by

$$L = 10 \lg \frac{\sum_{s=0}^{m} \sum_{i=0}^{n} \sum_{j=0}^{n} \sum_{k=0}^{n} \frac{QW_s}{4\pi d^2} * \delta * R * A * f}{10^{-12}} \quad \text{dB}, \qquad \text{for } i + j + k \leqslant n. \tag{8}$$

Here m is the number of sound sources, n is the reflection order, W_s is the sound power of the source, d is the distance travelled by the sound and δ determines if the sound strikes the barrier.

3. VALIDATION RESULTS

The predictions of the CISM and RAYCUB models were compared in three configurations of a laboratory space for the 2 kHz octave band, in an industrial space containing a single barrier for the octave bands 125 Hz to 4 kHz, and in a theoretical space with two configurations of absorptive patches.

3.1. THE LABORATORY SPACE INVESTIGATION

The laboratory space was a parallelepiped room 30 m long by 8 m wide by 3·85 m high, with an omnidirectional loudspeaker array located in the centre of one end of the room at a height of 0·85 m. Ten sound level measurements were taken along the central length of the room at a height of 1·5 m, for the 2 kHz octave band; see Figure 5. The floor was constructed of concrete ($\alpha = 0{\cdot}05$) and the wall material was formed from cellular concrete ($\alpha = 0{\cdot}1$). For more information concerning the laboratory space, see reference [2].

The three configurations of the space were as follows: Case 1, empty; Case 2, 40 blocks evenly distributed on the floor; Case 3, 240 fittings located in one half of the room. Each fitting was a polystyrene block ($\alpha = 0{\cdot}3$) of dimensions 0·5 m wide, 0·5 m long and 1 m high. The overall dimensions of the space and the layout of the fittings in the two fitted configurations are shown in Figure 5.

The geometry of the laboratory space was modelled as parallelepiped, with each of the six surfaces being allocated an appropriate absorption coefficient. In Cases 2 and 3 the fittings were modelled as a sub-volume or zone by both RAYCUB and CISM; the sound source was modelled as omnidirectional with an associated sound power level.

The receiver cells used in the RAYCUB model were cubic with a cell side length of 1 m. The number of reflections modelled, N, was defined by using an energy discontinuity percentage: that is, the percentage of energy which should be attenuated before the sound path is assumed to contribute negligibly to the overall sound level. An energy discontinuity of 99% was chosen as it has been shown to give the most accurate predictions in laboratory spaces [6]. The energy discontinuity percentage, P, is given as

$$N = \frac{\ln (1 - P/100)}{\ln (1 - \alpha_{av}) - hl}, \tag{9}$$

where α_{av} is the average absorption coefficient of the room, h is the air attenuation coefficient and l is the mean free path length of the space.

3.2. LABORATORY PREDICTIONS

For each of the three laboratory spaces, the performances of CISM and RAYCUB are presented in terms of average prediction difference (predicted minus measured sound level at each receiver position) to indicate the magnitude of the overall prediction accuracy and sound propagation (SP) curves (sound pressure level minus the sound power level); see Figures 6–8.

Case 1. The purpose of the empty space prediction was to demonstrate the accuracy of the CISM model in the simplest possible space. The predicted SP curves were similar to the measured curve (see Figure 6), giving an average prediction difference of 1·2 dB for CISM and 1·3 dB for RAYCUB. Hence, the CISM predictions were almost identical in shape and level to those predicted by RAYCUB. This indicated that the CISM model was accurate, and hence more complex spaces could be used in the investigation.

Case 2. The SP curve predicted by CISM was similar in shape and level to that predicted by RAYCUB; see Figure 7. This resulted in an average prediction difference of 0·8 dB for CISM and 1·2 dB for RAYCUB. The inaccuracy of CISM at the nearest receiver to the sound source was due to a lack of backscattering in the model which RAYCUB approximated by using the statistical random redirection of rays striking the fittings.

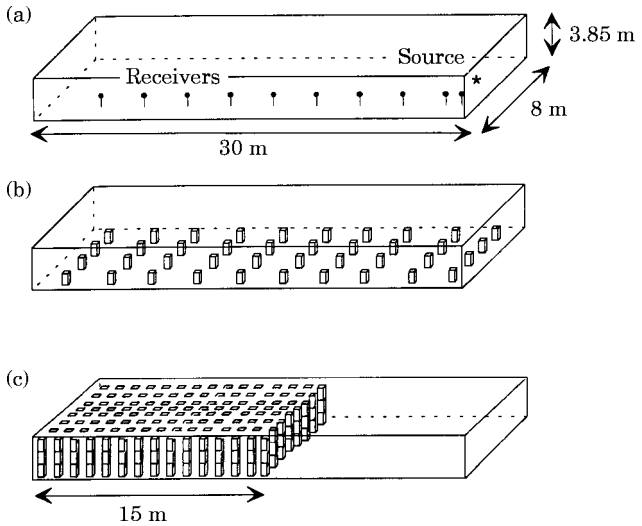

Figure 5. (a) The dimensions of the space and positions of the sound source and receivers in Cases 1, 2 and 3. (b) The configuration of the fittings in Case 2. (c) The configuration of the fittings in Case 3.

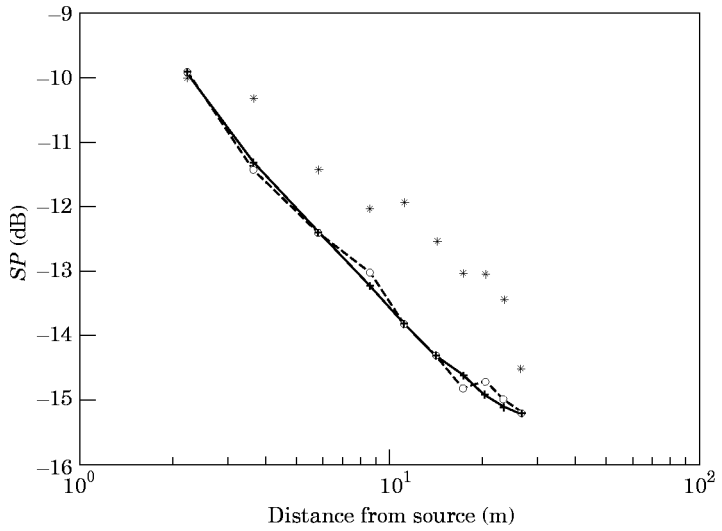

Figure 6. Measured (∗) and predicted by CISM (+) and RAYCUB (○) sound propagation in Case 1 ($q = 0$) for the 2 kHz octave band.

However, the actual difference between CISM and the measured sound level was small, showing that the backscattering effect was marginal.

Case 3. As in Case 2, the models approximately predicted the shape of the measured *SP* curve; see Figure 8. Again, CISM flattened the shape of the *SP* curve, due to the lack of backscattering which affected the predicted sound levels of the receivers directly in front of the fitted zone, resulting in an average prediction accuracy of 1·5 dB. RAYCUB was more accurate with an average prediction difference of 0·6 dB due to the prediction of the backscattering effect.

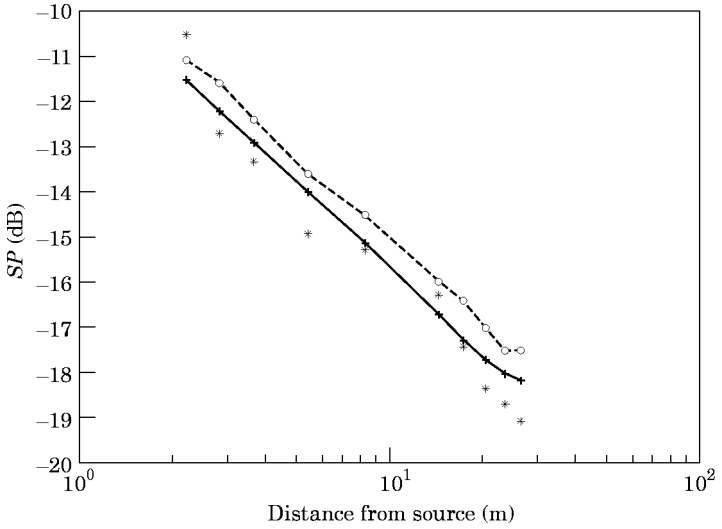

Figure 7. Measured (∗) and predicted by CISM (+) and RAYCUB (○) sound propagation in Case 2 ($q = 0{\cdot}09$) for the 2 kHz octave band.

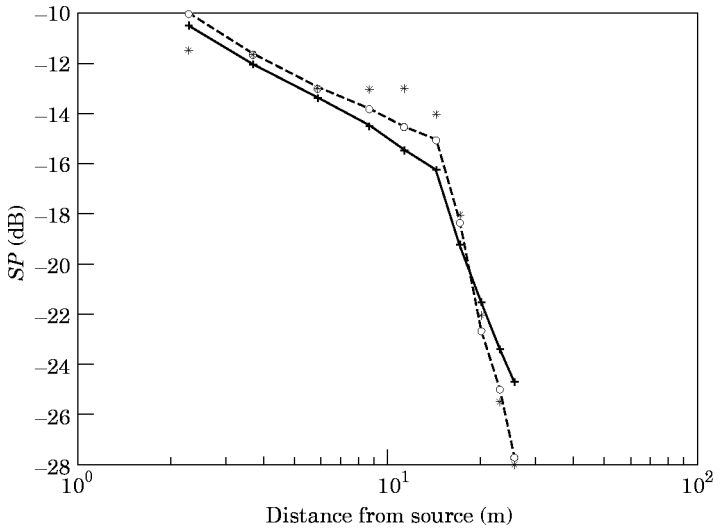

Figure 8. Measured (∗) and predicted by CISM (+) and RAYCUB (○) sound propagation in Case 3 ($q = 0{\cdot}56$) for the 2 kHz octave band.

The marginal increase in accuracy in Case 2 of RAYCUB compared with CISM, and the increase of less than 1 dB in Case 3, an extreme case, do not justify the inclusion of backscattering into the CISM model.

3.3. THE ABSORPTIVE PATCH INVESTIGATION

The theoretical investigation concerned the modelling of absorptive patches in two arrangements in a fictitious space. The first configuration, Case 4, had an arrangement of one patch centrally located on each room surface, whereas the second, Case 5, had a typical noise control approach of surrounding the sound source with absorptive materials, three patches located on the surfaces nearest the sound source; see Figure 9. The absorption coefficient of the absorptive patch was taken to be one minus the absorption coefficient

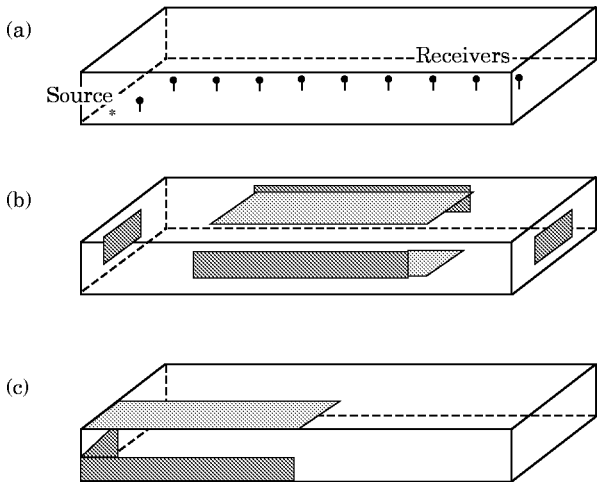

Figure 9. The theoretical space showing (a) positions of source and receivers, (b) centrally located patches, Case 4, and (c) noise control patch configuration, Case 5.

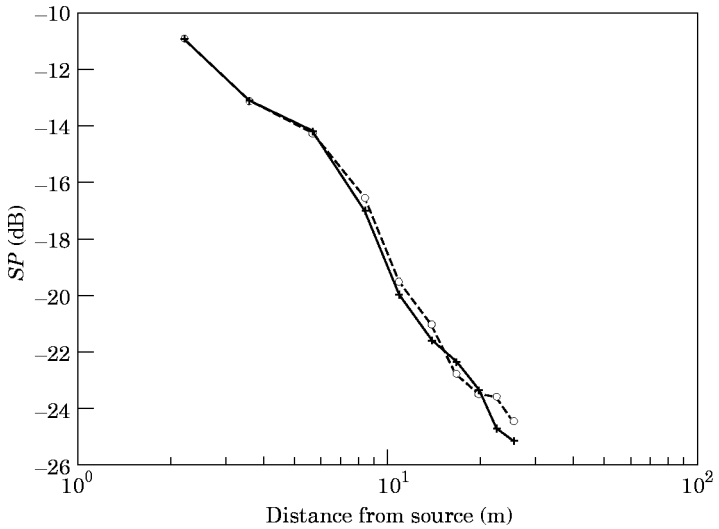

Figure 10. The CISM (+) and RAYCUB (○) predicted sound propagation in the theoretical space with arbitrary absorptive patches, Case 4.

of the room surface that it was located on; thus for the floor patch $\alpha = 0{\cdot}95$, for the ceiling patch $\alpha = 0{\cdot}85$ and for the wall patches $\alpha = 0{\cdot}9$.

It was considered important to model the exact location of the absorptive patches, as it has been shown that modelling patches by using an average technique over the room surfaces produces poor results both in terms of accuracy and *SP* shape [20]. The number of reflections used by CISM and RAYCUB was determined on the basis of a 99% energy discontinuity.

Case 4. Very similar *SP* curves both in shape and level were predicted by CISM and RAYCUB; see Figure 10.

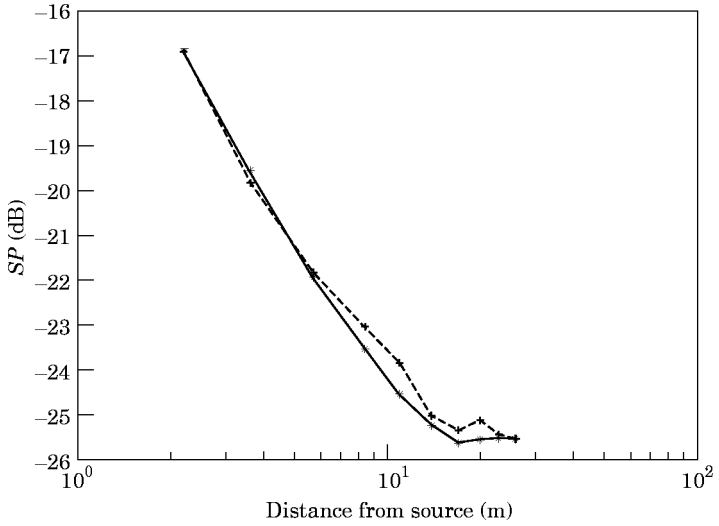

Figure 11. The CISM (+) and RAYCUB (○) predicted sound propagation in the theoretical space with noise control patches, Case 5.

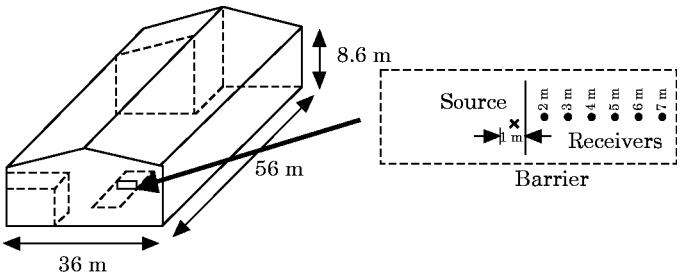

Figure 12. The empty factory space, showing the positions of the acoustic barrier, the source and the receivers.

Case 5. As can be seen from Figure 11 when compared to Figure 10, there was a 5 dB drop in the sound level predicted by both models compared to the previous predictions for the nearest receiver point to the sound source. As was seen in Case 4 the *SP* predictions of CISM and RAYCUB were very similar in both shape and level. For the furthest receiver positions from the sound source the predicted sound levels were the same as for Case 4, using only half the area of absorptive material.

3.4. THE BARRIER VALIDATION

Sound measurements were taken in an empty factory by Jones [21]. The space was 56 m long, 36 m wide and 8·6 m high, rising to a central apex of 10·6 m. The walls were constructed of brick, the ceiling was clad with 90 mm of rockwool backed with galvanized steel and faced with a perforated liner, and the floor was made of concrete. The factory was not fitted with machinery, but did contain steel skips set away from the measurement area. Sound measurements taken in the space demonstrated the existence of a non-diffuse sound field.

A barrier 2·7 m wide, 0·1 m deep and 2·4 m high was positioned centrally in the space; see Figure 12. The barrier was constructed from four interlocking panels. Each panel was formed from two layers of 0·05 m thick rockwool sandwiched between perforated hardboard and framed by a galvanized steel channel, to form a slab 0·9 m by 0·6 m by 0·1 m. The barrier performance was typical of this type of design; for the central octave bands 125 Hz to 4 kHz the calculated absorption coefficients based on reverberation-room measurements were as follows: 0·41, 0·96, 0·99, 0·89, 0·82 and 0·81.

The sets of measurements both with and without the barrier present were made in the factory space by using a Brüel and Kjaer Type 4224 sound source. The sound source showed a significant directivity pattern and hence RAYCUB-DIR and RAYCUB-DIR REDIR were used for the predictions rather than RAYCUB. Sound propagation measurements in the space were made for each of the octave bands 125 Hz to 4 kHz.

The sound source was positioned at a distance of 1 m directly in front of the barrier, at a height of 0·2 m. *SP* measurements were taken at six points one metre apart in the vicinity of the barrier; see Figure 12.

3.5. THE BARRIER PREDICTIONS

CISM represented the space as a parallelepiped of volume equal to that of the actual space, whereas the RAYCUB-DIR and RAYCUB-DIR REDIR models represented the exact geometry of the space. Both models used a 90% energy discontinuity, which has been found to be appropriate for industrial spaces [6].

TABLE 1

The averaged insertion loss prediction differences in the barrier investigation

	Frequency (Hz)					
	125	250	500	1k	2k	4k
RAYCUB-DIR	1·9	3·7	4·1	4·9	2·8	1·7
RAYCUB-DIR REDIR	1·0	1·6	2·3	3·3	1·7	1·9
CISM	1·8	3·3	2·8	4·0	2·5	0·9

For brevity, only three insertion loss (*IL*) graphs, at 125 Hz, 1 kHz and 4 kHz, are presented, in Cases 6, 7 and 8, respectively, see Figures 13–15. These were considered to be a representative sample of the results. Table 1 has been included for completeness, showing the average insertion loss prediction difference for each octave band, 125 Hz to 4 kHz.

Case 6. The relatively small insertion losses, 7–10 dB, measured at 125 Hz, suggested that a significant proportion of the sound was diffracted around the barrier. The RAYCUB-DIR REDIR model predicted the insertion losses accurately, giving a 1·0 dB average prediction difference. However, both CISM and RAYCUB-DIR failed to predict the reduced insertion loss directly beyond the barrier (see Figure 13), producing an average prediction difference of 1·8 dB and 1·9 dB, respectively. Hence, directly beyond the barrier sound diffracted around the barrier contributed 4 dB to the overall sound level, the insertion loss predicted by RAYCUB-DIR minus the measured insertion loss. Further from the sound source, the effect of the barrier diminished and hence all of the predictions became more accurate.

Case 7. The measured insertion losses at 1 kHz demonstrated an unusual shape due to the interference effects affecting the sound level when the measurements were taken in the absence of the barrier, which resulted in a flat sound propagation curve. This effect was ignored by the intensity based models: it would be necessary to use a pressure based

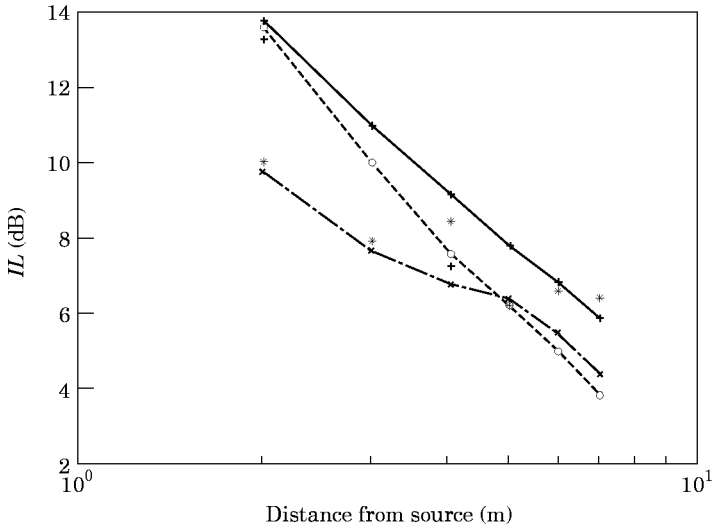

Figure 13. The measured (∗) and predicted CISM (+), RAYCUB-DIR (○) and RAYCUB-DIR REDIR (×) insertion loss in the empty factory space with barrier, Case 6, for the 125 Hz octave band.

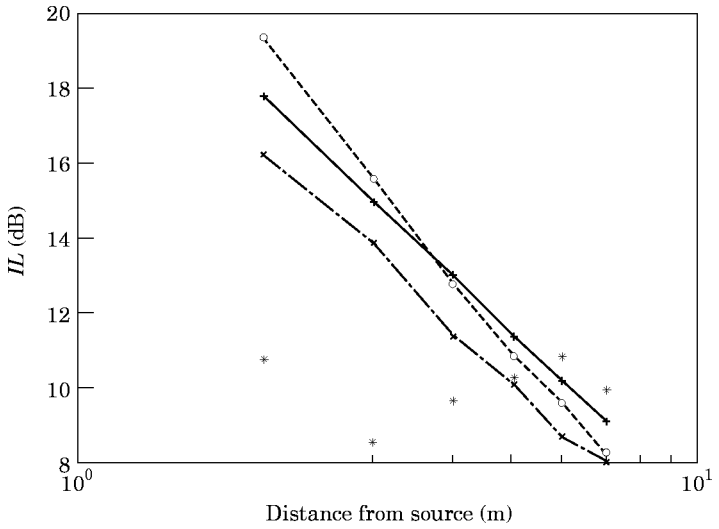

Figure 14. The measured (∗) and predicted by CISM (+), RAYCUB-DIR (○) and RAYCUB-DIR REDIR (×) insertion loss in the empty factory space with barrier, Case 7, for the 1 kHz octave band.

approach to model interference effects [12]. As a result, all of the models failed to predict accurately the insertion losses (see Figure 14), except for the furthest receiver positions where the reflected sound dominated the sound field. Overall, the insertion losses were predicted within approximately 4 dB of those measured.

Case 8. At 4 kHz the measured and predicted insertion losses were similar for all the models, and hence CISM predicted the insertion loss to within 0·9 dB on average, while the ray-tracing models RAYCUB-DIR and RAYCUB-DIR REDIR produced a 1·7 dB and 1·9 dB average prediction difference, respectively; see Figure 15. The diffraction model of RAYCUB-DIR REDIR had no significant effect at this high frequency and hence produced a similar prediction to RAYCUB-DIR. CISM produced accurate predictions at

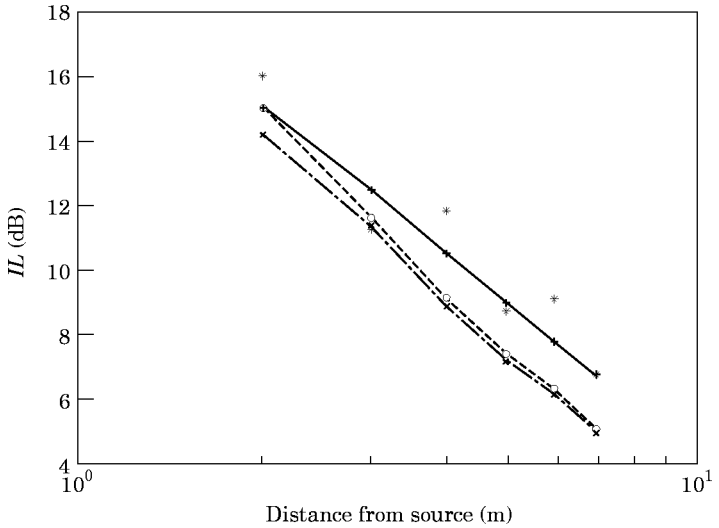

Figure 15. The measured (∗) and predicted by CISM (+), RAYCUB-DIR (○) and RAYCUB-DIR REDIR (×) insertion loss in the empty factory space with barrier, Case 8, for the 4 kHz octave band.

TABLE 2

The run-times (s) *and data file sizes* (*bytes*) *for the* RAYCUB, RAYCUB-DIR REDIR *and* CISM *models*

	RAYCUB		RAYCUB-DIR REDIR		CISM	
	Data size	Run-time	Data size	Run-time	Data size	Run-time
Case 2	672	10	672	2	153	2
Case 5	918	35	918	7	180	10
Case 7	732	40	1048	8	223	6
Factory	912	970	1696	194	835	16

higher frequencies as the acoustic barrier behaves as a totally sound absorbing barrier and geometrical considerations become increasingly important.

4. PERFORMANCE

The results presented in section 3 demonstrated that the predictions of CISM were as accurate as those of RAYCUB in spaces which included absorptive patches, uneven fitting distributions and acoustic barriers.

In Table 2 are presented the run-times (s) and data file size (bytes) for RAYCUB, RAYCUB-DIR, RAYCUB-DIR REDIR and CISM in some typical cases (Cases 2, 5 and 7) and in a previously predicted factory space [6]. An Intel Pentium IBM PC running at 90 MHz was used in all of the calculations presented.

Case 2. The original RAYCUB model was five times slower to execute than RAYCUB-DIR in the fitted laboratory space due to optimizations in the RAYCUB-DIR model; see Table 2. CISM was equally as fast as RAYCUB-DIR in this relatively small space, where it would be expected that the ray-tracing model would be quicker to execute. As the space was simple, all of the RAYCUB models represented the room identically, whereas CISM required less than one quarter of the data of RAYCUB.

Case 5. In the theoretical space with three absorptive patches, RAYCUB-DIR was marginally faster than CISM, due to the representation of patches adding significantly to the complexity of the model. Absorptive patches are more effectively modelled by CISM than RAYCUB, with CISM requiring one-fifth of the data of RAYCUB to describe the space fully.

Case 7. RAYCUB-DIR was slow to execute compared with CISM in the barrier space due to the large volume of the room. RAYCUB-DIR and RAYCUB-DIR REDIR used a different representation for the barrier, the latter requiring 40% more data than the former, so that the diffraction area around the barrier could be modelled. CISM represented the space using approximately one-quarter of the data used by the RAYCUB based models.

Factory spaces. Six factories were previously investigated: all were large and all were predicted using a 90% ED. Four of the six factories used multiple sound sources, between 13 and 21 sources, and the number of receivers, between 39 and 112, was also much greater than in the previous cases discussed. From Table 2 it can be seen that, for a typical factory, CISM calculated the sound distribution approximately 12 times faster than RAYCUB-DIR and 60 times faster than RAYCUB, achieving an average prediction accuracy of 2·0 dB as compared to 1·5 dB for RAYCUB-DIR. CISM required, on average, one half of the information of the RAYCUB-DIR model.

5. CONCLUSIONS

An image-source model, CISM, was developed on the basis of the predictions of RAYCUB, so that only the essential characteristics for representing a factory space were included. This allowed the model to execute quickly using the minimum amount of essential information, thus overcoming the main disadvantages of the RAYCUB model. The CISM model was designed to represent geometrically parallelepiped enclosed spaces with totally sound absorbing rectangular barriers and rectangular absorptive patches on the room surfaces. The fittings contained in the space could be represented as three volumes divided by parallel planes.

CISM was shown to predict accurately the sound propagation in a laboratory space configured as empty, floor-fitted and half-fitted. A theoretical space configured with arbitrarily positioned absorptive patches and patches located for optimal noise control was used to test the CISM model by comparison with the predictions of the RAYCUB model. CISM and RAYCUB predicted near identical sound propagation curves in both the arbitrary and noise control cases. By comparing the sound levels predicted for the arbitrary case with those of the noise control case, the advantage of a noise control approach was clearly demonstrated by the models.

In the barrier investigation, CISM predicted more accurately than RAYCUB-DIR in a complex space which the ray-tracing model could more accurately represent and geometrically model. This could be explained by the more precise nature of the image-source method compared to the ray-tracing technique. RAYCUB-DIR REDIR produced more accurate predictions, as this model incorporated an approximation for diffractional effects. However, incorporating a diffraction model into CISM would be cumbersome and impractical, defeating the advantages of the model.

CISM produced predictions as accurate as those of RAYCUB in the cases investigated, but did so using less information than required by RAYCUB, although the run-times were similar to those of RAYCUB-DIR. When the CISM and RAYCUB-DIR models were compared for typical industrial halls, CISM was 12 times faster than RAYCUB-DIR and used half of the information required by RAYCUB-DIR.

A demonstration version of CISM is available on the World Wide Web at http:\\www.sbu.ac.uk\ ~ acogrp\steve.html. The program requires Netscape 2.0 to run.

ACKNOWLEDGMENTS

The authors would like to thank the Institute National de Recherche et de Sécurité for providing the original RAYCUB model and the measurement data, and Dr Jones for allowing the use of her factory measurement data. This research was funded by the Engineering and Physical Sciences Research Council.

REFERENCES

1. M. Hodgson 1988 *Journal of the Acoustical Society of America* **84**, 253–261. On the prediction of sound fields in large empty rooms.
2. A. M. Ondet and J. L. Barbry 1989 *Journal of the Acoustical Society of America* **85**, 787–796. Modelling of sound propagation in fitted workshops using ray tracing.
3. M. Hodgson 1989 *Noise Control Engineering Journal* **33**, 97–104. Factory noise prediction using ray tracing—experimental validation and effectiveness of noise control measures.
4. H. A. Akil 1995 *Journal of Building Acoustics* **2**, 461–482. Determination of the scattering parameters of fittings in industrial buildings for use in computer based factory noise prediction models, part 1: theoretical background.

5. R. M. Windle 1994 *Proceedings of the Institute of Acoustics* **16**, 423–432. An independent comparison and validation of noise prediction techniques inside factories.
6. S. Dance 1993 *Ph.D. Thesis*, *South Bank University*. The development of computer models for the prediction of sound distribution in fitted non-diffuse spaces.
7. B. Gibbs and D. Jones 1972 *Acustica* **26**, 24–32. A simple image method for calculating the distribution of sound pressure levels within an enclosure.
8. S. Dance, J. Roberts and B. Shield 1995 *Journal of Building Acoustics* **1**, 125–136. Computer prediction insertion loss due to a single barrier in a non-diffuse empty enclosed space.
9. S. Jovicic 1979 *Work*, *Occupational Health and Social Affairs*, *Ministry of Rhenanie-Westpalie*, *Germany*. Recommendations for determination of sound level in industrial halls (in German).
10. E. Lindqvist 1982 *Acustica* **50**, 313–328. Sound attenuation in factory spaces.
11. U. Kurze 1985 *Journal of Sound and Vibration* **98**, 349–364. Scattering of sound in industrial spaces.
12. S. Dance, J. Roberts and B. Shield 1994 *Applied Acoustics* Computer prediction of sound distribution in enclosed spaces using an interference pressure model.
13. J. Borish 1984 *Journal of the Acoustical Society of America* **75**, 1827–1836. Extension of the image model to arbitrary polyhedra.
14. H. Lee and B.-H. Lee 1988 *Applied Acoustics* **24**, 87–115. An efficient model for the image model technique.
15. G. Lemire and J. Nicolas 1985 *Noise Control Engineering Journal* **24**, 58–67. Image method prediction of industrial hall noise levels—A new algorithm.
16. M. Hodgson 1990 *Journal of the Acoustical Society of America* **88**, 871–878. On the accuracy of models for predicting sound propagation in fitted rooms.
17. H. Kuttruff 1981 *Journal of the Acoustical Society of America* **69**, 1716–1723. Sound decay in reverberation chambers with diffusing elements.
18. W. Stahel and B. Braune 1977 *Inter-Noise* **77**, 105–112. Sound absorption and noise screens in large industrial halls.
19. E. Kotarbinska 1988 *Applied Acoustics* **23**, 99–109. How to calculate the efficiency of an acoustic barrier in a flat room.
20. S. Dance and B. Shield 1994 *Proceedings of the Institute of Acoustics* **16**, 515–524. Noise control modelling in non-diffuse enclosed spaces using an image-source model.
21. C. Jones 1990 *Ph.D. Thesis*, *South Bank Polytechnic*. Development of a computer model for prediction of sound fields in factory spaces.